KeAi

CHINESE ROOTS
GLOBAL IMPACT

#### Contents lists available at ScienceDirect

## Petroleum Science

journal homepage: www.keaipublishing.com/en/journals/petroleum-science



## Original Paper

## Similarities and differences in inherent mechanism and characteristic frequency between the one-dimensional poroelastic model and the layered White model



Li-Ming Zhao <sup>a</sup>, Cai-Ping Lu <sup>a, \*</sup>, Yang Liu <sup>a</sup>, Chao-Chao Li <sup>b</sup>

- <sup>a</sup> School of Mines, China University of Mining and Technology, Xuzhou, 221116, Jiangsu, China
- <sup>b</sup> Henan Institute of Geophysical Space Information, Zhengzhou, 450009, Henan, China

#### ARTICLE INFO

## Article history: Received 13 June 2023 Received in revised form 9 March 2024 Accepted 1 April 2024 Available online 4 April 2024

Edited by Jie Hao and Meng-Jiao Zhou

Keywords: 1D poroelastic model Layered White model Quasi-static flow Slow P-wave diffusion Characteristic frequency Diffusion length

#### ABSTRACT

The similarities and differences in inherent mechanism and characteristic frequency between the onedimensional (1D) poroelastic model and the layered White model were investigated. This investigation was conducted under the assumption that the rock was homogenous and isotropic at the mesoscopic scale. For the inherent mechanism, both models resulted from quasi-static flow in a slow P-wave diffusion mode, and the differences between them originated from saturated fluids and boundary conditions. On the other hand, for the characteristic frequencies of the models, the characteristic frequency of the 1D poroelastic model was first modified because the elastic constant and formula for calculating it were misused and then compared to that of the layered White model. Both of them moved towards higher frequencies with increasing permeability and decreasing viscosity and diffusion length. The differences between them were due to the diffusion length. The diffusion length for the 1D poroelastic model was determined by the sample length, whereas that for the layered White model was determined by the length of the representative elementary volume (REV). Subsequently, a numerical example was presented to demonstrate the similarities and differences between the models. Finally, published experimental data were interpreted using the 1D poroelastic model combined with the Cole-Cole model. The prediction of the combined model was in good agreement with the experimental data, thereby validating the effectiveness of the 1D poroelastic model. Furthermore, the modified characteristic frequency in our study was much closer to the experimental data than the previous prediction, validating the effectiveness of our modification of the characteristic frequency of the 1D poroelastic model. The investigation provided insight into the internal relationship between wave-induced fluid flow (WIFF) models at macroscopic and mesoscopic scales and can aid in a better understanding of the elastic modulus dispersion and attenuation caused by the WIFF at different scales.

© 2024 The Authors. Publishing services by Elsevier B.V. on behalf of KeAi Communications Co. Ltd. This is an open access article under the CC BY license (http://creativecommons.org/licenses/by/4.0/).

## 1. Introduction

Seismic wave propagating through shallow earth often undergoes significant dispersion and attenuation caused by intrinsic physical mechanisms in addition to scattering (e.g., Müller et al., 2010; Gurevich and Carcione, 2022; Chen et al., 2022, 2023a). These physical mechanisms are always influenced by the saturated fluid, the temperature and tectonic stress of the medium in which the wave propagates (e.g., Carcione et al., 2020; Chen et al., 2023b; Zong et al., 2023), and wave-induced fluid flow (WIFF) mechanism

is considered to be the main cause of the dispersion and attenuation in fluid-saturated rocks (e.g., Gurevich et al., 2010). WIFF refers to the fluid flow induced by the passing wave that creates pressure gradients within the fluid phase and is accompanied by internal friction until the fluid pressure get equilibrated (Müller et al., 2010). The WIFF can be categorized into macroscopic (global), mesoscopic and microscopic (local) flows in terms of the scale on which it occurs (Pride et al., 2004). Macroscopic flow occurs on a wavelength scale whereas microscopic flow occurs on a grain contact/pore size scale. Meanwhile, mesoscopic flow is supposed to take place on a scale much smaller than the prevailing wavelength but sufficiently larger than the typical pore size. All of them have been extensively investigated by theoretical models (e.g., Biot, 1941, 1956a, 1956b;

E-mail address: cplu@cumt.edu.cn (C.-P. Lu).

<sup>\*</sup> Corresponding author.

White, 1975; White et al., 1975; Mavko and Jizba, 1991; Vogelaar and Smeulders, 2007; Gurevich et al., 2009, 2010; Deng et al., 2012; Ba et al., 2016; Pimienta et al., 2016; Song et al., 2016; Chen et al., 2019; Sun et al., 2019; Tan et al., 2020; Zhao et al., 2022), numerical modeling (e.g., Quintal et al., 2011, 2016; Tisato and Quintal, 2013; Chen et al., 2018; He et al., 2023) and physical experiments (e.g., Plona, 1980; Batzle et al., 2006; Subramaniyan et al., 2015; Pimienta et al., 2015a, 2015b; Mikhaltsevitch et al., 2016; Yin et al., 2017; Ding et al., 2017; Chapman and Quintal, 2018; Li et al., 2020; Sun et al., 2022).

In the theoretical models for macroscopic flow, one important model is the one-dimensional (1D) poroelastic model, which is obtained by analytically solving the fluid pressure diffusion at the global scale. This model can govern the elastic modulus dispersion and attenuation from the drained state to the undrained state (i.e., drained/undrained transition) for fully-saturated rock samples (Pimienta et al., 2016). In the drained state, the pore fluid can flow freely in or out of the sample, and the elastic properties of the sample are similar to those under dry conditions. In the undrained state, the pore fluid has no time to flow out of the sample, and the pore pressure in the sample increases but remains isobaric. The undrained properties can be accurately predicted using the Gassmann formula (Gassmann, 1951). On the other hand, the White model is a mesoscopic WIFF model that is widely used to account for the elastic modulus dispersion and attenuation for partially saturated rock samples. The different fluids in the sample are distributed in patches (i.e., patchy saturation). The model was derived by extending the approach used by Gassmann and can be classified into the spherical White model (three-dimensional, 3D). which analyzes the response of gas pockets in a water-saturated porous medium, and the layered White model (1D), which considers the response of porous layers alternatively saturated with gas and water (White, 1975; White et al., 1975). Deng et al. (2012) rederived the layered White model based on Biot's consolidation equations (Biot, 1941) and obtained the same results as White et al. (1975). At a later time, Chapman and Quintal (2018) numerically modeled the patchy saturation in layers using the Biot's consolidation equations and the result showed exact consistence with the prediction of the layered White model, validating Deng et al. (2012)'s rederivation. Furthermore, Chapman and Quintal (2018) and Cao et al. (2019) also numerically modeled the drained/undrained transition based on Biot's consolidation equations, respectively, and both of the numerical results were in good agreement with the prediction of the 1D poroelastic model. The numerical results show that these two representative WIFF models at different scales (i.e., the 1D poroelastic model and the layered White model) are related to Biot's consolidation equations, suggesting that they are similar to each other. However, similarities between these two models have not vet been investigated. Do these two models originate from the same physical mechanism? Are there any differences between these two models?

To this end, we investigate the similarities and differences between these two representative WIFF models to reveal the internal relationship between them, and better understand the underlying mechanism and related modulus dispersion and attenuation. The investigation is conducted under the assumption that the rock is homogenous and isotropic at the mesoscopic scale. First, we briefly introduce the models. Then, we theoretically analyze the similarities and differences between them in terms of the inherent mechanism and characteristic frequency. In following section, we present a numerical example to demonstrate the similarities and the differences between the models. Finally, we compared the 1D poroelastic model with experimental data.

## 2. Theoretical backgrounds

## 2.1. The 1D poroelastic model

Based on the linear isotropic poroelastic theory, Zimmerman (2000) derived a partial derivative equation governing pore pressure  $(P_n)$  in a fluid-saturated homogenous medium:

$$\frac{\partial P_{p}}{\partial t} = \frac{\kappa B K_{d}}{\eta \alpha} \nabla^{2} P_{p} + B \frac{\partial P_{c}}{\partial t}, \tag{1}$$

where  $\kappa$  is the rock permeability, B is the Skempton coefficient,  $K_{\rm d}$  is the drained bulk modulus,  $\eta$  is the pore fluid viscosity,  $\alpha$  is the Biot coefficient, and  $P_{\rm c}$  is the confining pressure. The expressions for B and  $\alpha$  are (e.g., Zimmerman, 2000; Pimienta et al., 2016)

$$B = \frac{\frac{1}{K_{\rm d}} - \frac{1}{K_{\rm 0}}}{\frac{1}{K_{\rm d}} - \frac{1}{K_{\rm 0}} + \varphi\left(\frac{1}{K_{\rm f}} - \frac{1}{K_{\rm 0}}\right)},\tag{2}$$

$$\alpha = 1 - \frac{K_{\rm d}}{K_0},\tag{3}$$

where  $K_0$  is the grain bulk modulus,  $K_f$  is the pore fluid bulk modulus, and  $\varphi$  is the rock's porosity.

By assuming that the pore pressure  $P_p$  varies only with the z-axis, Pimienta et al. (2016) simplified Eq. (1) into a 1D case and obtained a 1D poroelastic model in the bulk modulus. In this study, we developed a 1D poroelastic model in terms of Young's modulus. In the 1D case, Eq. (1) can be simplified as follows:

$$\frac{\partial P_{p}}{\partial t} = \frac{\kappa B K_{d}}{\eta \alpha} \frac{\partial^{2} P_{p}}{\partial z^{2}} + \frac{B}{3} \frac{\partial P_{c}}{\partial t}, \tag{4}$$

For the drained/undrained transition, the pore fluid at both ends of the sample is connected to the atmosphere (Fig. 1), with the boundary condition of

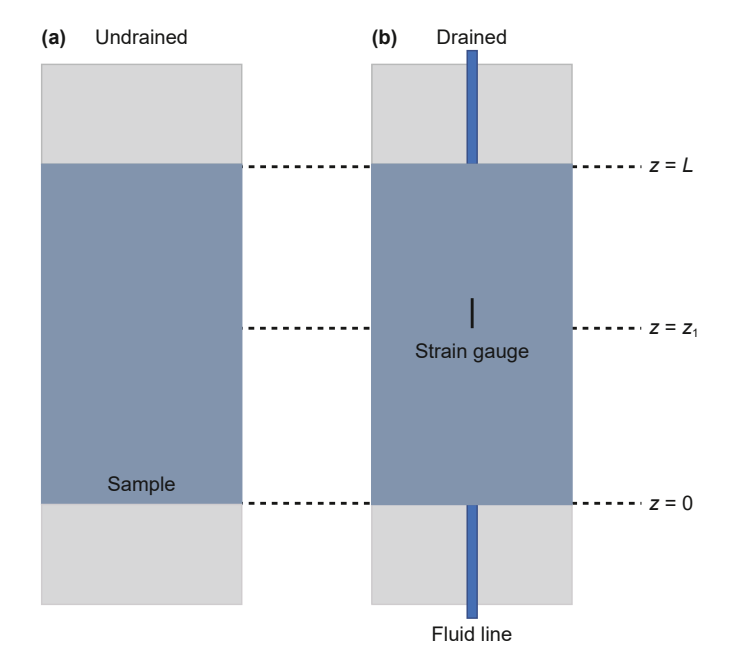


**Fig. 1.** Schematic of fluid-saturated rock sample with different states: **(a)** undrained state, **(b)** drained state.

$$P_{p}|_{z=0} = P_{p}|_{z=L} = 0, (5)$$

where *L* is the length of the sample.

With the time-harmonic confining pressure  $P_c$  (= $\Delta P e^{i\omega t}$ ,  $\Delta P$  is very small and close to a nil value, and  $\omega$  is the angular frequency), the solution to Eq. (4) is

$$P_{p}(z,t) = \frac{B}{3} \Delta P e^{i\omega t} \left[ 1 - \frac{\sinh(a(L-z)) + \sinh(az)}{\sinh(aL)} \right], \tag{6}$$

where the parameter  $a=(1+i)\sqrt{\frac{\alpha\omega\eta}{2B\kappa K_{\rm d}}}$  and other parameters are defined as before.

On the other hand, the axis strain is (Zimmerman, 2000)

$$\varepsilon_{\rm ax} = \frac{P_{\rm c}}{E_{\rm d}} - \frac{\alpha P_{\rm p}}{3K_{\rm d}},\tag{7}$$

where E<sub>d</sub> is the drained Young's modulus.

Subsequently, we obtained Young's modulus for the drained/undrained transition at the local position of the sample by

$$E = \frac{P_{\rm c}}{\varepsilon_{\rm ax}},\tag{8}$$

The Young's moduli and their corresponding attenuations at the sample scale (global scale) and strain gauge scale can be obtained by

$$E_{\rm gl} = \frac{P_{\rm c}}{\frac{1}{L} \int_{0}^{L} \varepsilon_{\rm ax}(z,t) dz},\tag{9a}$$

$$Q_{E-gl}^{-1} = \operatorname{Im}(E_{gl}) / \operatorname{Re}(E_{gl}), \tag{9b}$$

$$E_{\rm sg} = \frac{P_{\rm c}}{\frac{1}{l} \int_{z_{\rm r}}^{z_{\rm 1} + l} \varepsilon_{\rm ax}(z, t) \mathrm{d}z},\tag{10a}$$

$$Q_{\mathsf{F}-\mathsf{s}\sigma}^{-1} = \mathsf{Im}(E_{\mathsf{s}\mathsf{g}}) \ / \ \mathsf{Re}(E_{\mathsf{s}\mathsf{g}}), \tag{10b}$$

where  $E_{\rm gl}$  is the Young's modulus at the global scale,  $Q_{\rm E-gl}^{-1}$  is the corresponding attenuation at the global scale,  $E_{\rm sg}$  is the Young's modulus at the strain gauge scale,  $Q_{\rm E-sg}^{-1}$  is the corresponding attenuation at the strain gauge scale, l is the length of the strain gauge, and  $z_1$  is the starting point at which the strain gauge is bonded to the sample (Fig. 1).

## 2.2. The layered White model

White et al. (1975) initially developed a mesoscopic WIFF model to explain the elastic modulus dispersion and attenuation at seismic frequencies for partially saturated rocks (i.e., the layered White model, Appendix A). In the model, the partially saturated rock was assumed to be composed of porous layers alternatively saturated with gas and water (Fig. 2). Then, Deng et al. (2012) rederived the model using Biot's consolidation equations (Biot, 1941) (also called Biot's quasi-static equations of consolidation, Appendix B) and obtained the same results.

In the layered White model (Fig. 2), for each layer n (n = 1, 2) in the representative elementary volume (REV), the variation in the fluid pressure along the z-axis was derived using Eq. (B2–B4):

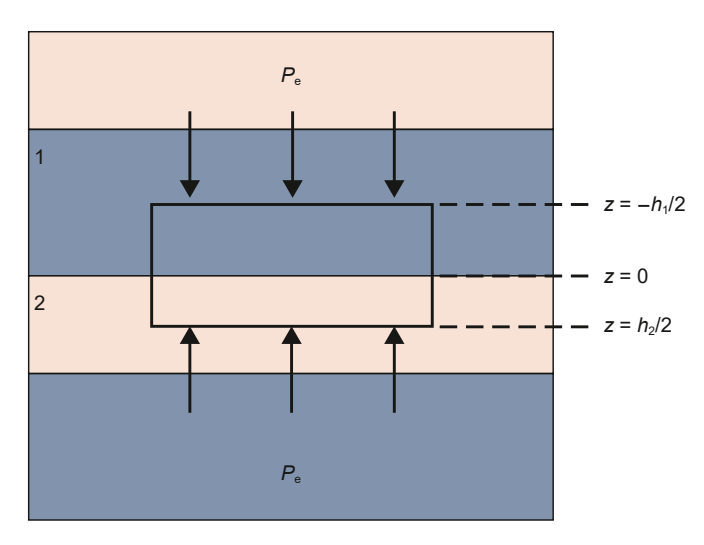


**Fig. 2.** Schematic of the layered White model: porous layers alternatively saturated with different fluids (gas and water). The porous layers saturated with different fluids in the black box represents the representative elementary volume (REV).

$$\frac{\partial P_{\rm f}}{\partial t} - D \frac{\partial^2 P_{\rm f}}{\partial z^2} = -r \frac{\partial \sigma_{zz}}{\partial t},\tag{11}$$

$$D = \frac{\kappa K_{\rm E}}{n},\tag{12}$$

where D is the diffusivity constant and the definition of parameters r, and  $K_F$  can be found in Appendix A.

To solve Eq. (11), the boundary conditions were (Deng et al., 2012)

$$\frac{\kappa}{\eta} \frac{\partial P_{f1}}{\partial z}|_{z=-h_1/2} = \frac{\kappa}{\eta} \frac{\partial P_{f2}}{\partial z}|_{z=h_2/2} = 0, \tag{13}$$

$$\frac{\kappa}{\eta} \frac{\partial P_{f1}}{\partial z}|_{z=0^{+}} = \frac{\kappa}{\eta} \frac{\partial P_{f2}}{\partial z}|_{z=0^{-}}, \tag{14}$$

$$P_{f1}|_{z=0^{+}} = P_{f2}|_{z=0^{-}}, (15)$$

where  $P_{f1}$  and  $P_{f2}$  are the fluid pressures in layers 1 and 2, respectively.

With the boundary conditions, Deng et al. (2012) obtained the complex P-wave modulus, which is the same as that in Eq. (A1). Furthermore, they derived analytical expressions for the fluid pressure, relative flow velocity of the pore fluid and frame displacement, providing more physical insights into the energy-loss mechanism associated with mesoscopic flow.

# 3. Similarities and differences in the inherent mechanism and characteristic frequency

## 3.1. The inherent mechanism

For the Biot consolidation equations (Appendix B), taking the divergence of both sides of Eq. (B2), we obtain

$$\frac{1}{M}\frac{\partial P_{f}}{\partial t} + \alpha \frac{\partial \varepsilon_{ii}}{\partial t} = \frac{\kappa}{n} \nabla^{2} P_{f}. \tag{16}$$

In addition, with the constitutive Eq. (B3), we can get

$$\sigma_{ii} = (2\mu_{\rm d} + 3\lambda_{\rm d})\varepsilon_{ii} - 3\alpha P_{\rm f},\tag{17}$$

Taking Eq. (17) into Eq. (16) gives

$$\left(\frac{1}{M} + \frac{\alpha^2}{K_d}\right) \frac{\partial P_f}{\partial t} + \frac{\alpha}{K_d} \frac{\partial^{\sigma_{ii}}}{\partial t} = \frac{\kappa}{\eta} \nabla^2 P_f, \tag{18}$$

Because  $P_{\rm c}=\frac{\sigma_{ii}}{3}$ , so Eq. (18) becomes

$$\left(\frac{1}{M} + \frac{\alpha^2}{K_d}\right) \frac{\partial P_f}{\partial t} + \frac{\alpha}{K_d} \frac{\partial P_c}{\partial t} = \frac{\kappa}{\eta} \nabla^2 P_f, \tag{19}$$

With the definition of  $\alpha$ , M, B, we can transform Eq. (19) into

$$\frac{\partial P_{\rm f}}{\partial t} = \frac{\kappa B K_{\rm d}}{\eta \alpha} \nabla^2 P_{\rm f} - B \frac{\partial P_{\rm c}}{\partial t}.$$
 (20)

Comparing Eqs. (1) and (20), it appears that the only difference between the two models is the sign of the second term on the right-hand side of the equations. However, the pore pressure in Zimmerman (2000) is negative for the fluid pressure in Biot (1941) and is the same as the fluid tension in Geertsma (1957) and White et al. (1975), so Eq. (1) becomes

$$\frac{\partial \left(-P_{\rm f}\right)}{\partial t} = \frac{\kappa B K_{\rm d}}{\eta \alpha} \nabla^2 \left(-P_{\rm f}\right) + B \frac{\partial P_{\rm c}}{\partial t},\tag{21a}$$

٥r

$$\frac{\partial P_{\rm f}}{\partial t} = \frac{\kappa B K_{\rm d}}{n \alpha} \nabla^2 P_{\rm f} - B \frac{\partial P_{\rm c}}{\partial t}, \tag{21b}$$

which is exactly equal to Eq. (20), indicating that both models are quasi-static models formed from the same quasi-static flow owing to fluid pressure diffusion. Furthermore, Chandler and Johnson (1981) demonstrated that the quasi-static flow owing to fluid pressure diffusion in Biot's consolidation equations is equivalent to Biot's slow P-wave. Therefore, both models exhibit a slow P-wave diffusion mode.

The differences between the two models are (1) the saturated fluid: there is one single fluid in the 1D poroelastic model, whereas there are two immiscible fluids in the layered White model, and (2) the boundary condition: the fluid can flow out at the ends of the sample in the 1D poroelastic model (i.e., Eq. (5)), whereas the fluid cannot flow out at the ends of the REV in the layered White model (i.e., Eq. (13)).

## 3.2. The characteristic frequency

Pimienta et al. (2015a) determined the characteristic frequency, that is, at which the attenuation peak appears, for the 1D poroelastic model (i.e., the drained/undrained transition) following Cleary (1978). The characteristic frequency  $f_c$  is (Pimienta et al., 2015a)

$$f_{\rm c} = \frac{d}{\left(\frac{L}{2}\right)^2},\tag{22}$$

where L/2 is the diffusion length, and d is the hydraulic diffusivity and defined by (Pimienta et al., 2015a)

$$d = K_{\rm d} \frac{\kappa}{\eta}, \tag{23}$$

Then, taking Eq. (23) into Eq. (22), they obtained (Pimienta et al., 2015a)

$$f_{\rm c} = \frac{4\kappa K_{\rm d}}{\eta L^2} \,. \tag{24}$$

However, in Cleary (1978), the hydraulic diffusivity is defined as

$$d = L_{\rm m} \frac{\kappa}{\eta},\tag{25}$$

where the parameter  $L_{\rm m}$  is an appropriate modulus of the fluidsaturated rock (Cleary, 1978). With the references of Müller et al. (2010) and Carcione (2015, section 7.13), for a diffusive wave, the parameter  $L_{\rm m}$  is determined by

$$L_{\rm m} = K_{\rm E}, \tag{26}$$

not the dry frame bulk modulus  $K_d$ . The parameter  $K_E$  is defined in Eq. (A9). Then, the hydraulic diffusivity d becomes the diffusivity constant D in Eqs. (11) and (12). Furthermore, the frequency related to the attenuation peak for the slow P-wave is (Brajanovski et al., 2006)

$$\omega_{\rm c} = \frac{2d}{\left(\frac{L}{2}\right)^2},\tag{27}$$

where  $\omega_{\rm c}=2\pi f_{\rm c}$  is an angular frequency. Thus, the characteristic frequency of the 1D poroelastic model is modified to be

$$f_{\rm c} = \frac{4\kappa K_{\rm E}}{\pi n L^2}.$$
 (28)

Meanwhile, the characteristic frequency of the layered White model is (Dutta and Seriff, 1979)

$$f_{\rm c}^{\rm White} = \frac{4\kappa K_{\rm E}}{\pi \eta (h_1 + h_2)^2}.$$
 (29)

where  $(h_1+h_2)/2$  is the total length of the REV in Fig. 2, which is also the diffusion length.

As both models are quasi-static models, Eqs. (28) and (29) show that the characteristic frequencies for the models are similar. Both move towards higher frequencies with increasing permeability and decreasing viscosity and diffusion length. However, the diffusion length for the 1D poroelastic model is determined by the length of the sample whereas that for the layered White model is determined by the length of the REV.

## 4. Numerical example

A numerical example was conducted to exhibit the similarities and differences in the inherent mechanism and characteristic frequency between the two models. As the drained/undrained transition is mainly captured by the dynamic stress-strain method in the laboratory, which always measures Young's modulus and its attenuation, we compared Young's modulus and its attenuation based on the two models. For the 1D poroelastic model, Young's modulus and its attenuation at the global and strain gauge scales are determined by Eqs. (9) and (10). For the layered White model, the Young's modulus and its attenuation is computed by

$$E_{\text{White}} = \text{Re}\left(\frac{3\mu_{\text{d}}P - 4\mu_{\text{d}}^2}{P - \mu_{\text{d}}}\right),\tag{30a}$$

$$Q_{\rm E}^{-1} = {\rm Im} \left( \frac{3\mu_{\rm d} P - 4\mu_{\rm d}^2}{P - \mu_{\rm d}} \right) / E_{\rm White}.$$
 (30b)

The physical parameters used in the numerical example are listed in Table 1. For the 1D poroelastic model, the sample is fully water-saturated with an open boundary condition, and Young's modulus and its attenuation at the global scale are computed. For the layered White model, the water saturation is about 99.9%, which is close to full saturation. The lengths of the REV  $(h_1+h_2)/2$ are 1.001L, 0.5005L and 0.250025L, respectively. The numerical results are shown in Fig. 3. When the diffusion lengths are approximately equal for the two models. Young's modulus and its attenuation are similar (black and red solid lines in Fig. 3). The insignificant difference between the two models is due to the different saturated fluids and boundary conditions. When the diffusion length of the layered White model becomes larger or smaller than that of the 1D poroelastic model, Young's modulus and its attenuation shift to lower or higher frequencies (red dotted lines) compared to that of the 1D poroelastic model.

In addition, when the diffusion lengths are approximately equal for the two models, the characteristic frequencies are about 25.8 Hz (the 1D poroelastic model) and 26.7 Hz (the layered White model), respectively, and are mostly equivalent to each other. When the diffusion length for the layered White model becomes smaller or larger, the corresponding frequencies are about 106.9 Hz and 6.7 Hz, respectively, which are higher or lower than that for the 1D poroelastic model. Moreover, when the diffusion lengths for both models are approximately equal, the characteristic frequency of the 1D poroelastic model predicted by Pimienta et al. (2015a) and our modified method are about 71.4 Hz and 25.1 Hz, respectively, showing that our modified characteristic frequency is closer to that of the numerical data.

## 5. Experimental data comparison

Pimienta et al. (2015a, 2015b) developed a new experimental setup to investigate the elastic modulus dispersion and attenuation at seismic frequencies when waves pass. For one sample that was fully saturated with water/glycerin, Young's modulus increased dramatically with increasing frequency, and two attenuation peaks appeared in the measured frequency range at an effective pressure

**Table 1**The physical parameters used in the numerical example.

Input parameters	Value
The bulk modulus of rock matrix $K_0$	37 GPa
The drained Young's modulus $E_d$	24 GPa
The drained Poisson's ratio $v_d$	0.15
The porosity $\varphi$	0.1
The permeability $\kappa$	10 mD
The length of the sample $L$	0.08 m
The bulk modulus of water $K_{\text{water}}$	2.25 GPa
The viscosity of water $\eta_{\text{water}}$	0.001 Pa·s
The bulk modulus of gas $K_{\rm gas}$	1 kPa
The viscosity of gas $\eta_{gas}$	1e−5 Pa·s
Confining oscillation amplitude $\Delta P$	0.2 MPa
The thickness of layer 1 $h_1$ (gas)	2L/1000, L/1000, L/2/1000
The thickness of layer 2 $h_2$ (water)	2L, L, L/2

of 1 MPa (Fig. 4). They attributed the first attenuation peak at lower frequencies to the drained/undrained transition, which is caused by macroscopic flow, and the other peak at higher frequencies to the undrained/unrelaxed transition, which is caused by microscopic flow (i.e., local/squirt flow). In the unrelaxed state, the pore fluid is unable to flow out of the sample, the pore pressure in the sample continue to increase from that of the undrained state, and it is no longer isobaric. They then interpreted the modulus dispersion and attenuation using the Zener viscoelastic model (Appendix C) combined with the Gassmann formula. The drained and unrelaxed Young's moduli are about 34 GPa and 65 GPa, respectively. The undrained Young's modulus was obtained by using the Gassmann formula. The characteristic frequencies for the macroscopic and microscopic flows are about 10 Hz and 1000 Hz, respectively (Pimienta et al., 2015b).

This interpretation phenomenally shows the frequency dependence of the modulus and its attenuation; however, it cannot reveal the underlying mechanism that controls the frequency dependence. Here, we use the 1D poroelastic model to interpret the first attenuation peak and its Young's modulus dispersion (at the strain gauge scale). The second attenuation peak and its Young's modulus dispersion cannot be interpreted using the classical squirt flow model (e.g., Gurevich et al., 2010) because of the lack of an important input parameter (microcrack's porosity). We here apply the Cole-Cole viscoelastic model (Appendix D) to explain the second attenuation peak and its Young's modulus dispersion (with the characteristic frequency of about 1000 Hz), which can cover the wide distribution in the aspect ratio of the rock's microcracks. The input parameters used in the 1D poroelastic model and the Cole-Cole model are listed in Table 2.

Fig. 4 shows the modeling results of the 1D poroelastic model and Cole-Cole model. In Fig. 4, for the first attenuation peak and its Young's modulus dispersion, the modeling result of the 1D poroelastic model shows the similar frequency-dependence trend with the measured data, and there is a slight discrepancy between the modeling result and the measured data. On the other hand, for the second attenuation and its Young's modulus dispersion, the modeling result of the Cole-Cole model is consistent with the measured data, suggesting that the aspect ratio of microcracks in natural rocks really has a wide distribution, not a single value. To explain the discrepancy between the modeling results and the measured data, especially the first attenuation peak, we combined the 1D poroelastic model and the Cole-Cole model to reinterpret the measured data. With Eqs. (10), (D1) and (D2), the real and imaginary parts of the complex modulus in the combined model are

$$\label{eq:energy_energy} \begin{split} E_{re} = E_{u} - \frac{1}{2} \left( E_{u} - \text{Re} \big( E_{sg} \big) \, \right) \bigg[ 1 - \frac{\text{sinh}(1-\beta)x}{\text{cosh}(1-\beta)x + \text{sin}(\beta x/2)} \bigg], \end{split} \tag{31a}$$

$$E_{\text{im}} = \frac{\frac{1}{2}(E_{\text{u}} - E_{\text{G}})\cos(\beta\pi/2)}{\cosh(1 - \beta)x + \sin(\beta x/2)} + \text{Im}(E_{\text{sg}}), \tag{31b}$$

where  $E_G$  is the undrained Young's modulus computed by the Gassmann formula and the Young's modulus  $E_{sg}$  is obtained by Eq. (10a). The corresponding attenuation is obtained by Eq. (D3). In Fig. 4, the modeling result of the combined model shows excellent agreement with the measured data, suggesting that the discrepancy between the modeling result of the 1D poroelastic model and the measured data is caused by the microscopic squirt flow with wide aspect ratio distribution and that the 1D poroelastic model

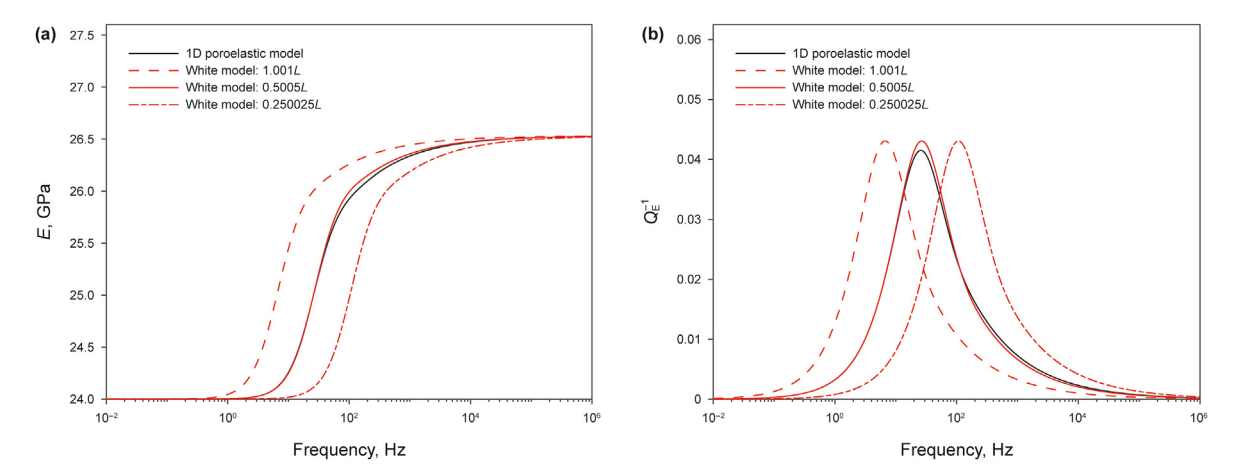


Fig. 3. Numerical results of the similarities and differences in the inherent mechanism and characteristic frequency between the two models.

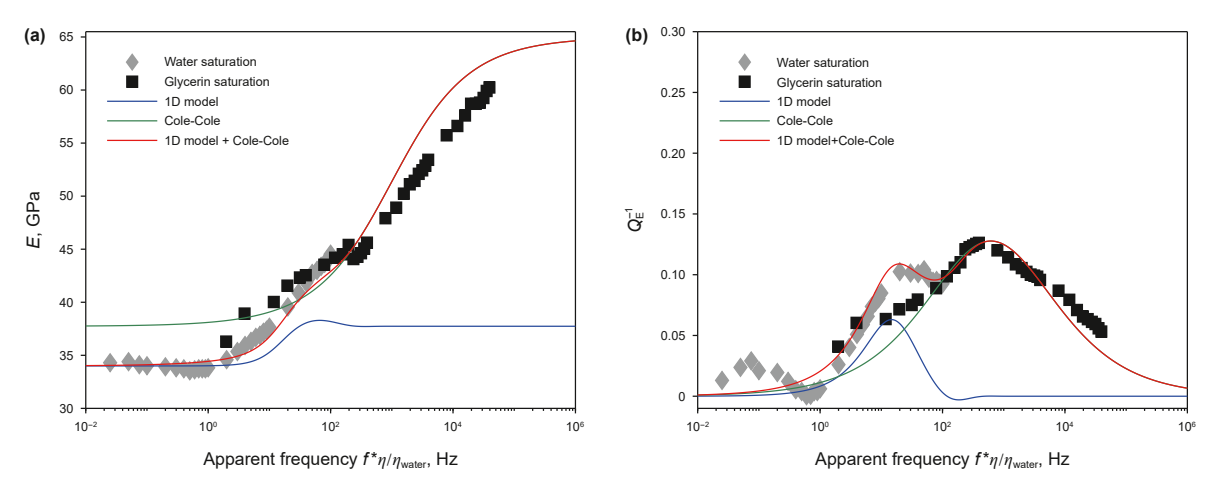


Fig. 4. Experimental data of Young's modulus and its attenuation from Pimienta et al. (2015b), and the modelling results of the 1D poroelastic model, Cole-Cole model, and their combined model

**Table 2**The input parameters used in the 1D poroelastic model and Cole-Cole model.

R		
Input parameters	Value	
The bulk modulus of rock matrix $K_0$	37 GPa	
The drained bulk modulus $K_d$	14 GPa	
The drained Young's modulus $E_{\rm d}$	34 GPa	
The unrelaxed Young's modulus $E_{\rm u}$	65 GPa	
The porosity $\varphi$	0.072	
The permeability $\kappa$	4 mD	
The length of the sample $L$	0.08 m	
The bulk modulus of water $K_{\text{water}}$	2.25 GPa	
The viscosity of water $\eta_{\text{water}}$	0.00089 Pa·s	
The viscosity of glycerin $\eta_{glycerin}$	0.35 Pa·s	
Confining oscillation amplitude $\Delta P$	0.2 MPa	
The starting point the strain gauge bonded on the sample $z_1$	0.037 m	
The length of strain gauge l	0.006 m	
β	0.44	

can predict the drained/undrained transition well.

On the other hand, in Fig. 4, the characteristic frequency of the drained/undrained transition in the measured data is about 20 Hz. Using Pimienta et al. (2015) 's method (i.e., Eq. (24)) and our modified method (i.e., Eq. (28)), the characteristic frequencies are predicted to be 39.3 Hz and 15.2 Hz, respectively. Compared with the measured characteristic frequency, our modified characteristic

frequency is much closer to the measured data, validating the effectiveness of the modification of the characteristic frequency of the 1D poroelastic model.

## 6. Conclusions

This study investigated the similarities and differences in the inherent mechanism and characteristic frequency between the 1D poroelastic model and the layered White model. Regarding the inherent mechanism, both models are derived from quasi-static flow due to fluid pressure diffusion and exhibits a slow P-wave diffusion mode. However, they have different saturated fluids and boundary conditions. On the other hand, for the characteristic frequency, the characteristic frequency of the 1D poroelastic model was first modified because the elastic constant  $L_{\rm m}$  and formula for calculating it were misused in Pimienta et al. (2015a), and then the characteristic frequencies for the models were compared. Both shift toward higher frequencies with increasing permeability and decreasing viscosity and diffusion length. The length of the sample determines the diffusion length for the 1D poroelastic model, whereas the length of the REV determines the diffusion length for the layered White model. Then, a numerical example was conducted to demonstrate the similarities and differences between the two models. The numerical results show that: (1) Young's modulus and its attenuation are similar when the diffusion lengths are

approximately equal to each other. The insignificant difference between the models is due to the different saturated fluids and boundary conditions. (2) When the diffusion length for the layered White model becomes larger or smaller than that for the 1D poroelastic model, Young's modulus and its attenuation shift to lower or higher frequencies, respectively, compared to that of the 1D poroelastic model. (3) The modified characteristic frequency is closer to that of the numerical data than the previous prediction by Pimienta et al. (2015a). Finally, the experimental data in Pimienta et al. (2015b) was reasonably interpreted using the 1D poroelastic model combined with the Cole-Cole model, validating the effectiveness of the 1D poroelastic model. Furthermore, the modified characteristic frequency is much closer to the experimental data than that of Pimienta et al. (2015a), validating the effectiveness of our modified characteristic frequency. This study revealed the internal relationship between the WIFF models at different scales and helped better understanding the elastic modulus dispersion and attenuation caused by them, thus having potential applications in analyzing seismic wave propagation in complex fluid-saturated porous subsurface.

## **CRediT** authorship contribution statement

**Li-Ming Zhao:** Methodology, Investigation, Project administration, Writing — original draft, Data curation, Formal analysis, Funding acquisition, Conceptualization. **Cai-Ping Lu:** Writing — review & editing, Supervision, Conceptualization, Methodology, Project administration. **Yang Liu:** Writing — review & editing, Data curation. **Chao-Chao Li:** Writing — review & editing, Investigation.

## **Declaration of competing interest**

The authors declare that they have no known competing financial interests or personal relationships that could have appeared to influence the work reported in this paper.

## Acknowledgement

This study is supported by the National Natural Science Foundation of China (42030810, 42104115). We are very grateful to the editors and the anonymous reviewers for their insightful comments that greatly enhanced the work.

#### Appendix A. The layered White model

In the layered White model, the complex P-wave modulus and its corresponding attenuation of the REV (Fig. 2) are computed by (White et al., 1975)

$$P = \frac{P_0}{1 + \frac{P_0(r_2 - r_1)^2}{i\omega(Z_1 - Z_2)(h_1 + h_2)}},\tag{A1a}$$

$$Q_P^{-1} = \operatorname{Im}(P) / \operatorname{Re}(P), \tag{A1b}$$

where

$$P_0 = \left(\frac{s_1}{P_{C1}} + \frac{s_2}{P_{C2}}\right),\tag{A2}$$

with  $s_n = h_n/(h_1 + h_2)$ , n = 1, 2, and

$$P_{\mathsf{G}n} = K_{\mathsf{G}n} + \frac{4}{3}\mu_{\mathsf{d}},\tag{A3}$$

where  $K_{Gn}$  is the undrained bulk modulus of the porous layer n (1, 2) computed by the Gassmann formula (Gassmann, 1951), and  $\mu_d$  is the drained shear modulus of the REV. The undrained bulk modulus  $K_{Gn}$  is obtained by

$$K_{Gn} = \frac{\varphi\left(\frac{1}{K_{fn}} - \frac{1}{K_0}\right) + \frac{1}{K_d} - \frac{1}{K_0}}{\frac{\varphi}{K_d}\left(\frac{1}{K_{fn}} - \frac{1}{K_0}\right) + \frac{1}{K_0}\left(\frac{1}{K_d} - \frac{1}{K_0}\right)},\tag{A4}$$

where  $K_{fn}$  (n = 1, 2) represents the bulk moduli of water and gas (or two immiscible fluids), respectively; and other parameters are defined as before.

The parameter  $r_n$  representing the ratio of fast P-wave fluid tension to total normal stress in the layer n (n = 1, 2) is given by

$$r_n = \frac{\alpha M_n}{P_{Gn}},\tag{A5}$$

with

$$\frac{1}{M_n} = \frac{\alpha - \varphi}{K_0} + \frac{\varphi}{K_{fn}}.\tag{A6}$$

The parameter  $Z_n$  representing the impedance related to the slow P-wave in the layer n is derived as

$$Z_n = \frac{\eta}{\kappa k_n} \coth\left(\frac{k_n h_n}{2}\right),\tag{A7}$$

where

$$k_n = \sqrt{\frac{i\omega\eta}{\kappa K_{\rm En}}},\tag{A8}$$

$$K_{\rm En} = \frac{P_{\rm d} M_n}{P_{\rm Gn}} \,, \tag{A9}$$

$$P_{\rm d} = K_{\rm d} + \frac{4}{3}\mu_{\rm d},\tag{A10}$$

where  $\kappa$  is the permeability of the REV (rock).

## Appendix B. Biot consolidation equations

The Biot's consolidation equations are given by (Biot, 1941; Quintal et al., 2011; Deng et al., 2012; Chapman and Quintal, 2018; He et al., 2023)

$$\nabla \cdot \boldsymbol{\sigma} = 0,\tag{B1}$$

$$\varphi\left(\frac{\partial \mathbf{u}}{\partial t} - \frac{\partial \mathbf{w}}{\partial t}\right) = \frac{\kappa}{n} \nabla P_{f},\tag{B2}$$

where  $\sigma$  is the total stress tensor with components  $\sigma_{ij}$ , i, j = x, y, z;  $\boldsymbol{u}$  is the vector of solid displacement with its components  $u_i$ ;  $\boldsymbol{w}$  is the vector of pore fluid displacement with its components  $w_i$ ; and  $P_f$  is the fluid pressure. The expressions for  $\sigma_{ij}$  and  $P_f$  (i.e., constitutive equations) are given by (e.g., Quintal et al., 2011; Deng et al., 2012)

$$\sigma_{ij} = 2\mu_{\rm d}\varepsilon_{ij} + \lambda_{\rm d}\varepsilon_{ii}\delta_{ij} - \alpha P_{\rm f}\delta_{ij},\tag{B3}$$

$$P_{\rm f} = M\zeta - \alpha M\varepsilon_{ii},\tag{B4}$$

$$\varepsilon_{ij} = \frac{1}{2} \left( \frac{\partial u_i}{\partial x_j} + \frac{\partial u_j}{\partial x_i} \right), \tag{B5}$$

where  $\mu_d$  and  $\lambda_d$  are the drained shear modulus and Lamé parameter, respectively;  $\delta_{ij}$  is the Kronecker delta;  $\zeta \equiv \varphi \nabla \cdot (\boldsymbol{u} - \boldsymbol{w})$  represents the volume of fluid which enters the pores of a unit volume of bulk material (Biot and Willis, 1957); the definition of parameter M can be found in Appendix A; and summation over repeated indices is implied.

## Appendix C. Zener model

The Zener model, which combines a spring in series with a parallel assemblage of a spring and dashpot (Mavko et al., 1998), is simple and straightforward. The frequency-dependent modulus and corresponding attenuation in the model are expressed as

$$M_{\rm re} = M_{\rm u} - \frac{M_{\rm u} - M_{\rm r}}{1 + (\omega \tau_0)^2},$$
 (C1)

$$Q_{\rm M}^{-1} = \Delta M \frac{\omega \tau_0}{1 + (\omega \tau_0)^2},\tag{C2}$$

$$\Delta M = \frac{M_{\rm u} - M_{\rm r}}{\sqrt{M_{\rm u} M_{\rm r}}},\tag{C3}$$

where  $M_{\rm u}$  is the unrelaxed modulus,  $M_{\rm r}$  is the relaxed/undrained modulus,  $\tau_0$  is relaxation time and given by  $\tau_0 = 1/(2\pi f_{\rm c})$ , and  $f_{\rm c}$  is the characteristic frequency.

## Appendix D. Cole-Cole model

In Zener model (i.e., Appendix C), the relaxation time is a single value. When the relaxation time changes from a single value to normally distributed values, which corresponds to different aspect ratios of soft pores/microcracks in natural rocks, the model becomes more general and is called the Cole-Cole model (Cole and Cole, 1941). The real and imaginary parts of the complex modulus in the model are

$$M_{re} = M_{u} + \frac{1}{2}(M_{r} - M_{u}) \left[ 1 - \frac{\sinh(1 - \beta)x}{\cosh(1 - \beta)x + \sin(\beta\pi/2)} \right], \tag{D1}$$

$$M_{\rm im} = \frac{\frac{1}{2}(M_{\rm u} - M_{\rm r})\cos(\beta\pi/2)}{\cosh(1 - \beta)x + \sin(\beta\pi/2)},$$
 (D2)

where the moduli  $M_{\rm u}$  and  $M_{\rm r}$  are defined as Appendix C, x is given by  $x=\ln(\omega\tau_0)$ , and  $\beta$  determines the width of the normal distribution of the relaxation time. When  $\beta=0$ , the relaxation time becomes a single value and the Cole-Cole model degenerates into the Zener model. The corresponding attenuation  $Q_{\rm M}^{-1}$  in the Cole-Cole model is obtained by

$$Q_{\rm M}^{-1} = \frac{M_{\rm im}}{M_{\rm re}}.$$
 (D3)

#### References

- Ba, J., Zhao, J.G., Carcione, J.M., et al., 2016. Compressional wave dispersion due to rock matrix stiffening by clay squirt flow. Geophys. Res. Lett. 43 (12), 6186–6195. https://doi.org/10.1002/2016GL069312.
- Batzle, M.L., Han, D.H., Hofmann, R., 2006. Fluid mobility and frequency-dependent seismic velocity—direct measurements. Geophysics 71 (1), N1–N9. https:// doi.org/10.1190/1.2159053.
- Biot, M.A., 1941. General theory of three-dimensional consolidation. J. Appl. Phys. 12 (2), 155–164. https://doi.org/10.1063/1.1712886.
- Biot, M.A., 1956a. Theory of propagation of elastic waves in a fluid-saturated porous solid. I. Low-frequency range. J. Acoust. Soc. Am. 28 (2), 168–178. https://doi.org/10.1121/1.1908239.
- Biot, M.A., 1956b. Theory of propagation of elastic waves in a fluid-saturated porous solid. II. Higher frequency range. J. Acoust. Soc. Am. 28 (2), 179–191. https:// doi.org/10.1121/1.1908241.
- Biot, M.A., Willis, D.G., 1957. The elastic coefficients of the theory of consolidation. J. Appl. Mech. 24 (4), 594–601. https://doi.org/10.1115/1.4011606.
- Brajanovski, M., Müller, T., Gurevich, B., 2006. Characteristic frequencies of seismic attenuation due to wave-induced fluid flow in fracture porous media. Geophys. J. Int. 166 (2), 574–578. https://doi.org/10.1111/j.1365-246X.2006.03068.x.
- Cao, C.H., Gurevich, B., Mikhaltsevitch, V., et al., 2019. Numerical simulation of the dead-volume effect in seismic-frequency measurements of elastic properties of fluid-saturated rocks. ASEG Ext. Abstr. 2019 (1), 1–3. https://doi.org/10.1080/ 22020586.2019.12073119.
- Carcione, J.M., 2015. Wave Fields in Real Media: Wave Propagation in Anisotropic, Anelastic, Porous, and Electromagnetic Media, third ed. Elsevier, Amsterdam.
- Carcione, J.M., Gei, D., Santos, J.E., et al., 2020. Canonical analytical solutions of wave-induced thermoelastic attenuation. Geophys. J. Int. 221 (2), 835–842. https://doi.org/10.1093/gji/ggaa033.
- Chandler, R.N., Johnson, D.L., 1981. The equivalence of quasistatic flow in fluid-saturated porous media and Biot's slow wave in the limit of zero frequency. J. Appl. Phys. 52 (5), 3391–3395. https://doi.org/10.1063/1.329164.
- Chapman, S., Quintal, B., 2018. Numerical analysis of local strain measurements in fluid-saturated rock samples submitted to forced oscillations. Geophysics 83 (5), MR309—MR316. https://doi.org/10.1190/geo2018-0071.1.
- Chen, F.B., Zong, Z.Y., Yin, X.Y., 2022. Acoustothermoelasticity for joint effects of stress and thermal fields on wave dispersion and attenuation. J. Geophys. Res. Solid Earth 127, e2021JB023671. https://doi.org/10.1029/2021JB023671.
- Chen, F.B., Zong, Z.Y., Yin, X.Y., et al., 2023a. Pressure and frequency dependence of elastic moduli of fluid-saturated dual-porosity rocks. Geophys. Prospect. 71, 1599–1615. https://doi.org/10.1111/1365-2478.13395.
- Chen, F.B., Zong, Z.Y., Stovas, A., et al., 2023b. Wave reflection and transmission coefficients for the layered transversely isotropic media with vertical symmetry axis under initial stress. Geophys. J. Int. 233 (3), 1580–1595. https://doi.org/ 10.1093/gji/ggad011.
- Chen, H., Gilbert, R.P., Guyenne, P., 2018. A Biot model for the determination of material parameters of cancellous bone from acoustic measurements. Inverse Probl. 34 (8), 1. https://doi.org/10.1088/1361-6420/aac520.
- Chen, H., Gilbert, R.P., Guyenne, P., 2019. Dispersion and attenuation in a porous viscoelastic model for gravity waves on an ice-covered ocean. Eur. J. Mech. B Fluid 78, 88–105. https://doi.org/10.1016/j.euromechflu.2019.06.002.
- Cleary, M.P., 1978. Elastic and dynamic response regimes of fluid impregnated solids with diverse microstructures. Int. J. Solid Struct. 14 (10), 795–819. https://doi.org/10.1016/0020-7683(78)90072-0.

- Cole, K.S., Cole, R.H., 1941. Dispersion and absorption in dielectrics I. Alternating current Characteristics. J. Chem. Phys. 9 (4), 341–351. https://doi.org/10.1063/ 1.1750906.
- Deng, J.X., Wang, S.X., Du, W., 2012. A study of the influence of mesoscopic pore fluid flow on the propagation properties of compressional waves—a case of periodic layered porous media. Chin. J. Geophys. 55 (8), 2716–2727. https://doi.org/10.6038/j.issn.0001-5733.2012.08.024 (in Chinese).
- Ding, P.B., Di, B.R., Wang, D., et al., 2017. Measurements of seismic anisotropy in synthetic rocks with controlled crack geometry and different crack densities. Pure Appl. Geophys. 174 (5), 1907–1922. https://doi.org/10.1007/s00024-017-1520-3.
- Dutta, N.C., Seriff, A.J., 1979. On White's model of attenuation in rocks with partial gas saturation. Geophysics 44 (11), 1806—1812. https://doi.org/10.1190/1.1440940.
- Gassmann, F., 1951. Über die elastizität poröser medien. Vierteljahrsschrift der Naturforschenden Gesellschaft Zürich 96, 1—23.
- Geertsma, J., 1957. The effect of fluid pressure decline on volumetric changes of porous rocks. Transactions of the AIME 210 (1), 331–340. https://doi.org/ 10.2118/728-G.
- Gurevich, B., Makarynska, D., Pervukhina, M., 2009. Ultrasonic moduli for fluid-saturated rocks: Mavko-Jizba relations rederived and generalized. Geophysics 74 (4), N25–N30. https://doi.org/10.1190/1.3123802.
- Gurevich, B., Makarynska, D., Paula, O.B., et al., 2010. A simple model for squirt-flow dispersion and attenuation in fluid-saturated granular rocks. Geophysics 75 (6), 109–120. https://doi.org/10.1190/1.3509782.
- Gurevich, B., Carcione, J.M., 2022. Attenuation and Dispersion of Elastic Waves in Porous Rocks: Mechanisms and Models. Society of Exploration Geophysicists,
- He, Y.X., He, W.T., Zhang, W.F., et al., 2023. Sensitivity of seismic attenuation and dispersion to dynamic elastic interactions of connected fractures: quasi-static finite element modeling study. Petrol. Sci. 20 (1), 177–198. https://doi.org/ 10.1016/j.petsci.2022.08.024.
- Li, H., Wang, D.X., Gao, J.H., et al., 2020. Role of saturation on elastic dispersion and attenuation of tight rocks: an experimental study. J. Geophys. Res. Solid Earth 125 (4), e2019JB018513. https://doi.org/10.1029/2019JB018513.
- Mavko, G., Mukerji, T., Dvorkin, J., 1998. The Rock Physics Handbook: Tools for Seismic Analysis in Porous Media. Cambridge University Press, New York.
- Mavko, G., Jizba, D., 1991. Estimating grain-scale fluid effects on velocity dispersion in rocks. Geophysics 56 (12), 1940—1949. https://doi.org/10.1190/1.1443005.
- Mikhaltsevitch, V., Lebedev, M., Gurevich, B., 2016. Laboratory measurements of the effect of fluid saturation on the elastic properties of carbonates at seismic frequencies. Geophys. Prospect. 64 (4), 799–809. https://doi.org/10.1111/1365-2478.12404.
- Müller, T., Gurevich, B., Lebedev, M., 2010. Seismic wave attenuation and dispersion resulting from wave-induced flow in porous rocks—a review. Geophysics 75 (5), 75A147—75A164. https://doi.org/10.1190/1.3463417.
- Plona, T.J., 1980. Observation of a second bulk compressional wave in a porous medium at ultrasonic frequencies. J. Appl. Phys. 36 (4), 259–261. https://doi.org/10.1063/1.91445.
- Pimienta, L., Fortin, J., Guéguen, Y., 2015a. Bulk modulus dispersion and attenuation in sandstones. Geophysics 80 (2), D111–D127. https://doi.org/10.1190/GEO2014-03351
- Pimienta, L., Fortin, J., Guéguen, Y., 2015b. Experimental study of Young's modulus dispersion and attenuation in fully saturated sandstones. Geophysics 80 (5), L57–L72. https://doi.org/10.1190/geo2014-0532.1.

- Pimienta, L., Borgomano, J.V.M., Fortin, J., et al., 2016. Modelling the drained/undrained transition: effect of the measuring method and the boundary conditions. Geophys. Prospect. 64 (4), 1098–1111. https://doi.org/10.1111/1365-2478 12390
- Pride, S.R., Berryman, J.G., Harris, J.M., 2004. Seismic attenuation due to wave-induced flow. J. Geophys. Res. Solid Earth 109 (B1), B01201. https://doi.org/10.1029/2003/B002639.
- Quintal, B., Steeb, H., Frehner, M., et al., 2011. Quasi-static finite element modeling of seismic attenuation and dispersion due to wave-induced fluid flow in porcelastic media. J. Geophys. Res. Solid Earth 116 (1), B01201. https://doi.org/ 10.1029/20101B007475.
- Quintal, B., Rubino, J.G., Caspari, E., et al., 2016. A simple hydromechanical approach for simulating squirt-flow type. Geophysics 81 (4), D335—D344. https://doi.org/10.1190/GF02015-0383.1.
- Subramaniyan, S., Quintal, B., Madonna, C., et al., 2015. Laboratory-based seismic attenuation in Fontainebleau sandstone: evidence of squirt flow. J. Geophys. Res. Solid Earth 120 (11), 7526—7535. https://doi.org/10.1002/2015JB012290.
- Song, Y., Hu, H.S., Rudnicki, J.W., 2016. Dynamic bulk and shear moduli due to grainscale local fluid flow in fluid-saturated cracked poroelastic rocks: theoretical model. J. Mech. Phys. Solid. 92, 28–54. https://doi.org/10.1016/ j.jmps.2016.03.019.
- Sun, C., Tang, G.Y., Zhao, J.G., et al., 2019. Three-dimensional numerical modeling of the drained/undrained transition for frequency-dependent elastic moduli and attenuation. Geophys. J. Int. 219 (1), 27–38. https://doi.org/10.1093/gji/ggz284.
- Sun, C., Fortin, J., Borgomano, J.V.M., et al., 2022. Influence of fluid distribution on seismic dispersion and attenuation in partially saturated limestone. J. Geophys. Res. Solid Earth 127 (5), 1–22. https://doi.org/10.1029/2021JB023867.
- Tan, W.H., Müller, T.M., Ba, J., et al., 2020. Drained-to-undrained transition of bulk

- modulus in fluid-saturated porous rock induced by dead volume variation. Geophys. Prospect. 68 (8), 2494–2503. https://doi.org/10.1111/1365-2478.13002.
- Tisato, N., Quintal, B., 2013. Measurements of seismic attenuation and transient fluid pressure in partially saturated Berea sandstone: evidence of fluid flow on the mesoscopic scale. Geophys. J. Int. 195 (1), 342–351. https://doi.org/10.1093/gji/ggt259.
- Vogelaar, B., Smeulders, D., 2007. Extension of White's layered model to the full frequency range. Geophys. Prospect. 55 (5), 685–695. https://doi.org/10.1111/ j.1365-2478.2007.00648.x.
- White, J.E., 1975. Computed seismic speeds and attenuation in rocks with partial gas saturation. Geophysics 40 (2), 224–232. https://doi.org/10.1190/1.1440520.
- White, J.E., Mikhaylova, N.G., Lyakhovitskiy, F.M., 1975. Low-frequency seismic waves in fluid-saturated layer rocks. J. Acoust. Soc. Am. 57 (su1), 1935–1937. https://doi.org/10.1121/1.1995164, 1975.
- Yin, H.J., Zhao, J.G., Tang, G.Y., et al., 2017. Pressure and fluid effect on frequency-dependent elastic moduli in fully saturated tight sandstone. J. Geophys. Res. Solid Earth 122 (11), 8925–8942. https://doi.org/10.1002/2017JB014244.
- Zhao, L.M., Chen, T.J., Mukerji, T., 2022. Brown and Korringa's expression for the saturated bulk modulus at high frequencies: modification of Mavko and Jizba's squirt flow model. Geophysics 87 (4), MR201–MR208. https://doi.org/10.1190/geo2021-0496.1.
- Zimmerman, R., 2000. Coupling in poroelasticity and thermoelasticity. Int. J. Rock Mech. Min. 37 (1), 79–87. https://doi.org/10.1016/S1365-1609(99)00094-5.
- Zong, Z.Y., Chen, F.B., Yin, X.Y., 2023. Effect of stress on wave propagation in fluid-saturated porous thermoelastic media. Surv. Geophys. 44, 425–462. https://doi.org/10.1007/s10712-022-09743-y.